Use of dMLC for implementation of dynamic respiratory-gated radiation therapy

Eric W. Pepin[a)] and Huanmei Wu
Purdue School of Engineering Technology, IUPUI, Indianapolis, Indiana 46202

Hiroki Shirato
Hokkaido University School of Medicine, Sapporo 060-8638, Japan

(Received 17 March 2013; revised 10 August 2013; accepted for publication 21 August 2013; published 13 September 2013)

Purpose: To simulate and evaluate the use of dynamic multileaf collimators (dMLC) in respiratory gating to compensate for baseline drift.
Methods: Tumor motion tracking data from 30 lung tumors over 322 treatment fractions was analyzed with the finite state model. A dynamic respiratory gating window was established in real-time by determining the average positions during the previous two end-of-expiration breathing phases and centering the dMLC aperture on a weighted average of these positions. A simulated dMLC with physical motion constraints was used in dynamic gating treatment simulations. Fluence maps were created to provide a statistical description of radiation delivery for each fraction. Duty cycle was also calculated for each fraction.
Results: The average duty cycle was 2.3% greater under dynamic gating conditions. Dynamic gating also showed higher fluences and less tumor obstruction. Additionally, dynamic gating required fewer beam toggles and each delivery period was longer on average than with static gating.
Conclusions: The use of dynamic gating showed better performance than static gating and the physical constraints of a dMLC were shown to not be an impediment to dynamic gating. © *2013 American Association of Physicists in Medicine*. [http://dx.doi.org/10.1118/1.4820534]

Key words: lung cancer, respiratory motion, respiratory gating, baseline shift

1. INTRODUCTION

The treatment of lung tumors with radiation therapy has long been hampered by respiratory induced tumor motion.[1] One clinical technique often used to compensate for the motion, and at the same time avoid larger treatment margins,[2–4] is respiratory gating. This image-guided procedure aims to irradiate the tumor only when it is in a predefined spatial window, i.e., the gating window.[5,6] The benefits of respiratory gating are primarily applied to lung treatments, but have also yielded successes with liver[7] and breast treatments.[8] The trade-off when using respiratory gating is a decrease in treatment margins, but an increase in treatment session duration.[4,9,10]

In order to accurately deliver the prescribed dose in a gated treatment, the tumor motion needs to be reproducible so that the gating window is frequently occupied. As such, the treatment window is often defined based on the tumor position in the end of expiration (EOE) phase of the breathing cycle.[3,10,11] The reproducibility of the EOE phase[11,12] is aided by its long duration compared to the inhalation peak and the slowness of tumor motion within the phase.[2,12] However, the reproducibility of EOE gating is still hindered by the phenomenon of baseline-shift,[8,11,13] in which the intrafraction motion of the EOE tumor position renders the predefined gating window inaccurate.

The use of dynamic multileaf collimators (dMLCs) has been investigated since the 1990s[14,15] and has been in wide use since[16] then because it allows for greater tumor conformality and increased avoidance of organs at risk while treating from multiple gantry angles.[17,18] With further technological advancements, dMLCs have been made possible such treatment methods as intensity modulated radiation therapy (IMRT) (Ref. 19–21) and arc therapies.[22–24] Recent research has investigated using dMLCs and tumor tracking systems to couple IMRT with motion compensation.[25–28] George *et al.* used dynamic tracking and breathing coaching to reduce treatment margins, but found some errors to be robust with free breathing and real-time tracking.[29] Trofimov *et al.* attempted to compensate for slow drifts during gated IMRT, detecting such changes in 12–15 s, resulting in an increased duty cycle.[30] Yoon *et al.* also used a moving average to specifically account for tumor motion perpendicular to the direction of MLC leaf travel.[31] They found this increased efficiency and reduced dosimetric errors, but with γ-test values still outside the passing criteria of $\leq$3%. In all applications of dMLC, it is necessary to note the mechanical restrictions on the leaf motion.[32,33] Numerous studies have determined maximum leaf velocities ranging from 0.5 to 4.0 cm/s,[17,34–37] with the more recent studies suggesting a value close to 3 cm/s, which will be used in this study. Restrictions on leaf acceleration have been described as negligible, however, one study determined a range of 46–69 cm/s^2;[35] this study will use 50 cm/s^2.

Our previous investigation developed a method of dynamic respiratory gating to compensate EOE baseline-shift[38] based on the finite state model (FSM) by Wu[39] which can identify the EOE phase of the tracked motion in real-time during treatment delivery. In this technical note, we will simulate an

application of that method to evaluate the feasibility of using a dMLC to make the adjustments necessary for dynamic respiratory gating in a real-time tracking scenario with free breathing.

2. METHODS AND MATERIALS

2.A. Materials

This study used the 3D motion of implanted gold fiducials in 30 lung tumors during 322 radiotherapy fractions tracked using four orthogonal fluoroscopes in real-time at a rate of 30 Hz at Hokkaido University.[40] The 3D respiratory motion data was categorized into four breathing states: expiration (EX), EOE, inhalation (IN), and irregular (IRR), based on the FSM.

A virtual model of a dMLC was created that consisted of two banks of 60 leaves; the central 40 leaves in each bank had a width of 5 mm at isocenter and the peripheral 20 had a width of 10 mm at isocenter. The leaves were modeled as having finite velocity and acceleration, but infinite jerk.

2.B. Methods

2.B.1. Tumor motion stimulation and modeling

Tumor motion was simulated as a 1 cm ($V = 4.2$ cm^3) rigid sphere centered on the motion data points from the tracking database fed in an online fashion. To simulate the dMLC treatment, the beam eye view (BEV) is set as the SI-LAT plane. The amplitude of 2D motion in the BEV was defined as the maximum Cartesian separation between tumor positions in the IN and EOE peaks. For the data set, the average amplitude was 7.8 mm ($\sigma = 5.1$). The intrafraction baseline drift was defined as the maximum separation between any two EOE peaks in a given fraction. For our data set, the average baseline drift was 3.3 mm ($\sigma = 2.3$).

2.B.2. Gating window determination

The initial location of the dMLC aperture was set as the average tumor position during the first EOE segment, which was monitored with closed leaves (Fig. 1). This aperture was opened for the second breathing cycle. Following the second breathing cycle, the aperture was adjusted to a weighted-average of two previous EOE breathing phases with a 0.95/0.05 weighting per our previous investigation,[38] with the 0.95 weighting going to the more recent EOE phase. These two cycles constitute the pretreatment learning phase. The aperture size was established by expanding the representative tumor body by a 2 mm margin in the BEV. The dMLC leaves were then directed to move so that the midpoint of the leading edge of each leaf was on this expanded tumor radius. If the leading edge midpoint was outside this margin, the leaves were directed to close at the midline.

Simulations were run that considered two styles of gating:

- Static gating: The dMLC aperture was fixed at the end of the pretreatment learning phase and not adjusted for the duration of the treatment fraction.
- Dynamic gating: The dMLC was used to adjust the aperture at the end of each EOE phase after the pretreatment learning phase according to the 0.95/0.05 weighting scheme.

The duty cycle was calculated as the fractional time during which the tumor was in the aperture, i.e., the tumor origin was within 2 mm of the aperture center.

2.B.3. dMLC motion

For each mode of gating, static, and dynamic, three models of dMLC motion were simulated to evaluate the impact of physical motion limitations:

1. Infinite maximum leaf speed and infinite leaf acceleration.

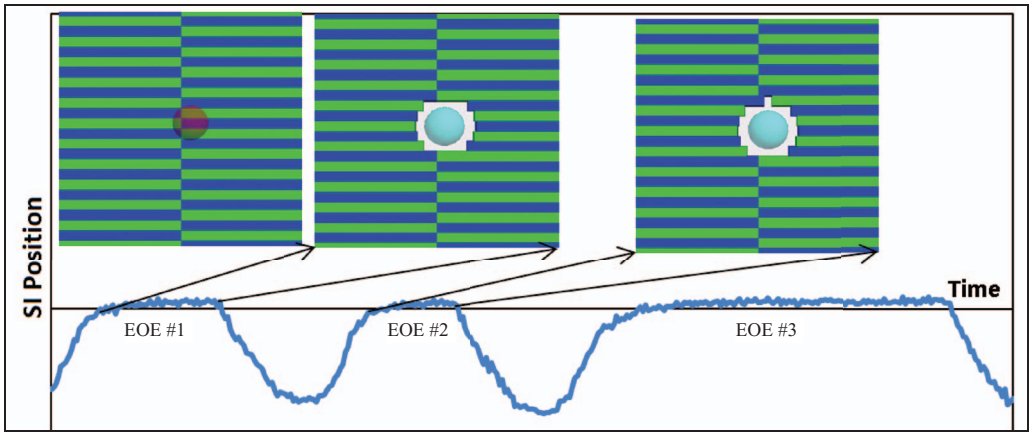

FIG. 1. Example of dMLC gating. This figure shows the motion trace of the first three breathing cycles of a sample patient and the corresponding dMLC shapes during the treatment fraction. During the first breathing cycle the dMLC is closed. In subsequent EOE phases, the dMLC opening is informed primarily by the previous EOE phase. The graphical representations of the tumor and dMLC are placed above the EOE phases to which they correspond. The arrows indicate the motion data that are predominantly informing the location of the dMLC aperture. The change in tumor color indicates that it is recognized as being within the aperture, so radiation is being delivered.

2. Finite maximum leaf speed (3 cm/s) and infinite leaf acceleration.
3. Finite maximum leaf speed (3 cm/s) and finite leaf acceleration (50 cm/s^2).

Leaf motion commenced upon the tumor's exit from each EOE phase and continued until the new position of the aperture was achieved per Sec. 2.B.2.

2.B.4. Evaluation metrics

During each fraction, the BEV tumor projection was pixelated so that the relative fluence could be determined throughout the tumor. This matrix was used to determine the average fraction of the target that was obstructed by the MLC leaves during each delivery segment.

The number of beam-on/beam-off toggle cycles, which are caused by the tumor entering and exiting the dMLC aperture, was determined for each fraction, as well as the duration of each visit in the aperture of the tumor. Average values of these statistics were compared for static and dynamic gating. Due to variations in fraction length and individual breathing patterns, comparisons were made on a per fraction basis and the average percent variation was calculated.

3. RESULTS

The average duty cycle for all treatment fractions when using the dynamic gating window was 51.6%, compared to 49.3% for the static gating window. This difference (2.3%) was significant ($p < 0.01$), however, 117 of the 322 fractions (36%) had a higher duty cycle with the static window. The average fluence to the tumor was increased by 13.4% ($p < 0.01$) when using dynamic gating compared to static gating. The minimum and maximum fluences were increased by 15.7% ($p < 0.01$) and 12.5% ($p < 0.01$), respectively. It is important to note that the duty cycle is independent of the physical parameters limiting dMLC leaf motion; differences due to these parameters are in Table I.

Static gating resulted in an average of 4.8 more beam toggles per fraction than dynamic gating (109.9 vs 105.1, $p < 0.01$, two-tailed, paired). However, when considering the relative difference in beam toggles when using static or dynamic gating on a per fraction basis, the difference was no significant (95% CI = [−0.78, 0.76]). Similarly, that the beam-on/beam-off cycles were, on average, 16.9% longer with dynamic gating than static gating did not achieve significance (95% CI = [−1.14, 0.08]).

4. DISCUSSION

Several ambiguities and potential contradictions in the results warrant brief discussion.

First, in Sec. 3, it is reported that in a minority of cases the duty cycle was greater when using a static gating window. This phenomenon was discussed at length in our previous work,[38] but briefly, it is due to smaller amplitudes of tumor motion resulting in occupancy of the gating window for breathing phases other than EOE. A hypothesized consequence of transient window occupation during phases other than EOE was an increased number of beam toggles and a shorter duration of such cycles due to the tumor completely passing through the aperture between inspiration and expiration peaks. This was not conclusively observed as there were mixed results for intertumor comparisons and interfraction comparisons of individual tumors. A more in depth investigation into how this result correlates with motion amplitude and sharpness of FSM phase transition is warranted.

Second, the fluence matrix is of little use in evaluating the alterations in dose caused by this technique. It was developed as a surrogate for partial obstruction of the tumor by dMLC leaves. While dynamic gating showed a smaller average fractional obstruction, this difference, 0.1%–0.2%, was not significant. This result is countered by the average fluence being 13.4% higher when using dynamic versus static gating. The apparent discrepancy is resolved by recognizing the dependency of average fractional obstruction on the maximum fluence, which is 12.5% higher on average with dynamic versus static gating. These methods can be improved in subsequent research by using Monte Carlo simulation or physical experimentation to investigate dose as well as fluence.

Third, the various physical leaf parameters can be seen to affect several metrics. The fixed width of the leaves limits the ability to shape the aperture. This can negatively impact dose delivery to the target if portion of the leaf inside the gating coordinates obscured an off-center target; this would be most

TABLE I. Comparison of fluence results for 1 cm tumor radius. This table shows how the fluence calculation was affected by the introduction of physical limitations on dMLC leaf motion. Analyses of variance showed that the differences in average fraction obstruction were significant for both dynamic and static gating ($F > 110$, $F_{crit} = 3$ and $F > 31$, $F_{crit} = 3$, respectively), whereas the fluence reductions were not ($F < 0.01$, $F_{crit} = 3$, and $F < 0.01$, $F_{crit} = 3$, respectively). For rows 1–3, columns 3 and 5 are to be read in reference to columns 1 and 4, respectively, and columns 3 and 6 are to be read in reference to columns 2 and 5, respectively.

	Dynamic gating			Static gating		
Leaf motion characteristics	$v = \infty$; $a = \infty$	$v = 3$ cm/s; $a = \infty$	$v = 3$ cm/s; $a = 50$ cm/s^2	$v = \infty$; $a = \infty$	$v = 3$ cm/s; $a = \infty$	$v = 3$ cm/s; $a = 50$ cm/s^2
Reduction in average fluence	…	0.48%	0.02%	…	0.57%	0.02%
Reduction in minimum fluence	…	1.21%	0.01%	…	1.41%	0.01%
Reduction in maximum fluence	…	0%	0.09%	…	0%	0.09%
Average fractional obstruction	0%	0.5%	0.4%	0%	0.6%	0.5%

likely with the most superior or inferior open leaf pair or first closed pair, but was not observed in the investigation. The finite width can also increase normal tissue irradiation as might occur in EOE #3 in Fig. 1. An error in targeting, e.g., poorly predicting the next EOE location, will not negatively impact dosimetry because irradiation only occurs when the tumor location matches the window coordinates. A targeting error will, however, reduce the duty cycle. The leaf motion parameters do have the potential to reduce dose delivery to the target in the event that the tumor returns to the gating window coordinates before the leaves have established the corresponding aperture.

Finally, the addition of leaf acceleration as a parameter was a novel component of this investigation. The consistent finding that this inclusion only introduced an additional 0.02% deficiency relative to modeling with infinite acceleration suggests that it may be possible to exclude it from future models in order to decrease computation times.

5. CONCLUSION

A study investigated the efficacy of making baseline adjustments in dynamic respiratory gating treatments using a dMLC in real-time. Dynamic gating significantly outperformed static gating in the metrics of duty cycle, maximum fluence, average fluence, and beam toggling. While not significant, dynamic gated also tended to obstruct the target less often. These results suggest that dMLC may be a practical way to improve the efficiency of respiratory gated radiation therapy.

ACKNOWLEDGMENTS

This research was supported in part by NIH Grant No. 1R21CA130849-01A.

[a]Author to whom correspondence should be addressed. Electronic mail: epepin@slu.edu

[1]R. Li, J. H. Lewis, L. I. Cervino, and S. B. Jiang, "A feasibility study of markerless fluoroscopic gating for lung cancer radiotherapy using 4DCT templates," Phys. Med. Biol. **54**, N489–N500 (2009).
[2]R. Muirhead, C. Featherstone, A. Duffton, K. Moore, and S. McNee, "The potential clinical benefit of respiratory gated radiotherapy (RGRT) in non-small cell lung cancer (NSCLC)," Radiother. Oncol. **95**, 172–177 (2010).
[3]A. Tai, J. D. Christensen, E. Gore, A. Khamene, T. Boettger, and X. A. Li, "Gated treatment delivery verification with on-line megavoltage fluoroscopy," Int. J. Radiat. Oncol., Biol., Phys. **76**, 1592–1598 (2010).
[4]C. Nelson, P. Balter, R. C. Morice, K. Bucci, L. Dong, S. Tucker, S. Vedam, J. Y. Chang, and G. Starkschall, "Evaluation of tumor position and PTV margins using image guidance and respiratory gating," Int. J. Radiat. Oncol., Biol., Phys. **76**, 1578–1585 (2010).
[5]K. Ohara, T. Okumura, M. Akisada, T. Inada, T. Mori, H. Yokota, and M. J. Calaguas, "Irradiation synchronized with respiration gate," Int. J. Radiat. Oncol., Biol., Phys. **17**, 853–857 (1989).
[6]C. G. Willett, R. M. Linggood, M. A. Stracher, M. Goitein, K. Doppke, D. C. Kushner, T. Morris, J. Pardy, and R. Carroll, "The effect of the respiratory cycle on mediastinal and lung dimensions in Hodgkin's disease. Implications for radiotherapy gated to respiration," Cancer **60**, 1232–1237 (1987).
[7]E. Yorke, K. E. Rosenzweig, R. Wagman, and G. S. Mageras, "Interfractional anatomic variation in patients treated with respiration-gated radiotherapy," J. Appl. Clin. Med. Phys. **6**, 19–32 (2005).
[8]S. Korreman, A. Pedersen, T. Nottrup, L. Specht, and H. Nystrom, "Breathing adapted radiotherapy for breast cancer: Comparison of free breathing gating with the breath-hold technique," Radiother. Oncol. **76**, 311–318 (2005).
[9]H. Liu, N. Koch, G. Starkschall, M. Jacobson, K. Forster, Z. Liao, R. Komaki, and C. Stevens, "Evaluation of internal lung motion for respiratory-gated radiotherapy using MRI: Part II—Margin reduction of internal target volume1," Int. J. Radiat. Oncol., Biol., Phys. **60**, 1473–1483 (2004).
[10]R. W. Underberg, J. R. van Sornsen de Koste, F. J. Lagerwaard, A. Vincent, B. J. Slotman, and S. Senan, "A dosimetric analysis of respiration-gated radiotherapy in patients with stage III lung cancer," Radiat. Oncol. **1**, 8 (2006).
[11]Y. Cui, J. G. Dy, B. Alexander, and S. B. Jiang, "Fluoroscopic gating without implanted fiducial markers for lung cancer radiotherapy based on support vector machines," Phys. Med. Biol. **53**, N315–N327 (2008).
[12]N. M. Wink, M. Chao, J. Antony, and L. Xing, "Individualized gating windows based on four-dimensional CT information for respiration-gated radiotherapy," Phys. Med. Biol. **53**, 165–175 (2008).
[13]P. R. Poulsen, B. Cho, D. Ruan, A. Sawant, and P. J. Keall, "Dynamic multileaf collimator tracking of respiratory target motion based on a single kilovoltage imager during arc radiotherapy," Int. J. Radiat. Oncol., Biol., Phys. **77**, 600–607 (2010).
[14]C. S. Chui, S. Spirou, and T. LoSasso, "Testing of dynamic multileaf collimation," Med. Phys. **23**, 635–641 (1996).
[15]G. Loi, E. Pignoli, M. Scorsetti, V. Cerreta, A. Somigliana, R. Marchesini, A. Gramaglia, U. Cerchiari, and S. B. Ricci, "Design and characterization of a dynamic multileaf collimator," Phys. Med. Biol. **43**, 3149–3155 (1998).
[16]M. Nielsen, J. Carl, and J. Nielsen, "A phantom study of dose compensation behind hip prosthesis using portal dosimetry and dynamic MLC," Radiother. Oncol. **88**, 277–284 (2008).
[17]Y. Liang, H. Xu, J. Yao, Z. Li, and W. Chen, "Four-dimensional intensity-modulated radiotherapy planning for dynamic multileaf collimator tracking radiotherapy," Int. J. Radiat. Oncol., Biol., Phys. **74**, 266–274 (2009).
[18]P. Keall, H. Cattell, D. Pokhrel, S. Dieterich, K. Wong, M. Murphy, S. Vedam, K. Wijesooriya, and R. Mohan, "Geometric accuracy of a real-time target tracking system with dynamic multileaf collimator tracking system," Int. J. Radiat. Oncol., Biol., Phys. **65**, 1579–1584 (2006).
[19]S. Webb and D. M. Binnie, "A strategy to minimize errors from differential intrafraction organ motion using a single configuration for a 'breathing' multileaf collimator," Phys. Med. Biol. **51**, 4517–4531 (2006).
[20]P. Vial, L. Oliver, P. B. Greer, and C. Baldock, "An experimental investigation into the radiation field offset of a dynamic multileaf collimator," Phys. Med. Biol. **51**, 5517–5538 (2006).
[21]M. Shaikh, J. Burmeister, M. Joiner, S. Pandya, B. Zhao, and Q. Liu, "Biological effect of different IMRT delivery techniques: SMLC, DMLC, and helical tomotherapy," Med. Phys. **37**, 762 (2010).
[22]P. Zygmanski, W. Högele, R. Cormack, L. Chin, and R. Löschel, "A volumetric-modulated arc therapy using sub-conformal dynamic arc with a monotonic dynamic multileaf collimator modulation," Phys. Med. Biol. **53**, 6395–6417 (2008).
[23]J. Zimmerman, S. Korreman, G. Persson, H. Cattell, M. Svatos, A. Sawant, R. Venkat, D. Carlson, and P. Keall, "DMLC motion tracking of moving targets for intensity modulated arc therapy treatment—A feasibility study," Acta Oncol. **48**, 245–250 (2009).
[24]P. R. Poulsen, B. Cho, A. Sawant, and P. J. Keall, "Implementation of a new method for dynamic multileaf collimator tracking of prostate motion in arc radiotherapy using a single kV imager," Int. J. Radiat. Oncol., Biol., Phys. **76**, 914–923 (2010).
[25]L. Papiez, R. McMahon, and R. Timmerman, "4D DMLC leaf sequencing to minimize organ at risk dose in moving anatomy," Med. Phys. **34**, 4952–4956 (2007).
[26]R. McMahon, R. Berbeco, S. Nishioka, M. Ishikawa, and L. Papiez, "A real-time dynamic-MLC control algorithm for delivering IMRT to targets undergoing 2D rigid motion in the beam's eye view," Med. Phys. **35**, 3875–3888 (2008).
[27]R. McMahon, L. Papiez, and G. Sandison, "Addressing relative motion of tumors and normal tissue during dynamic MLC tracking delivery," Australas. Phys. Eng. Sci. Med. **30**, 331–336 (2007).

[28]B. Cho, P. R. Poulsen, A. Sloutsky, A. Sawant, and P. J. Keall, "First demonstration of combined kV/MV image-guided real-time dynamic multileaf-collimator target tracking," Int. J. Radiat. Oncol., Biol., Phys. **74**, 859–867 (2009).
[29]R. George, J. Williamson, M. Murphy, E. Weiss, and P. Keall, "On the accuracy of a moving average algorithm for tracking respiratory motion during radiation therapy treatment delivery," Med. Phys. **33**, 2356–2365 (2006).
[30]A. Trofimov, C. Vrancic, T. C. Y. Chan, G. Sharp, and T. Bortfield, "Tumor trailing strategy for IMRT in the presence of target motion: Preliminary studies," Med. Phys. **34**, 1718–1733 (2007).
[31]J. W. Yoon, A. Sawant, Y. Suh, B. C. Cho, T. S. Suh, and P. Keall, "Experimental investigation of a moving averaging algorithm for motion perpendicular to the leaf travel direction in dynamic MLC target tracking," Med. Phys. **38**, 3924–3931 (2011).
[32]D. Rangaraj and L. Papiez, "Synchronized delivery of DMLC intensity modulated radiation therapy for stationary and moving targets," Med. Phys. **32**, 1802–1817 (2005).
[33]L. Papiez and R. M. Abolfath, "Variable beam dose rate and DMLC IMRT to moving body anatomy," Med. Phys. **35**, 4837–4848 (2008).
[34]P. R. Poulsen, B. Cho, A. Sawant, D. Ruan, and P. J. Keall, "Detailed analysis of latencies in image-based dynamic MLC tracking," Med. Phys. **37**, 4998–5005 (2010).
[35]K. Wijesooriya, C. Bartee, J. V. Siebers, S. S. Vedam, and P. J. Keall, "Determination of maximum leaf velocity and acceleration of a dynamic multileaf collimator: Implications for 4D radiotherapy," Med. Phys. **32**, 932–941 (2005).
[36]R. McMahon, L. Papiez, and D. Rangaraj, "Dynamic-MLC leaf control utilizing on-flight intensity calculations: A robust method for real-time IMRT delivery over moving rigid targets," Med. Phys. **34**, 3211–3223 (2007).
[37]J. R. McClelland, S. Webb, D. McQuaid, D. M. Binnie, and D. J. Hawkes, "Tracking 'differential organ motion' with a 'breathing' multileaf collimator: Magnitude of problem assessed using 4D CT data and a motion-compensation strategy," Phys. Med. Biol. **52**, 4805–4826 (2007).
[38]E. W. Pepin, H. Wu, and H. Shirato, "Dynamic gating window for compensation of baseline shift in respiratory-gated radiation therapy," Med. Phys. **38**, 1912–1918 (2011).
[39]H. Wu, G. C. Sharp, B. Salzberg, D. Kaeli, H. Shirato, and S. B. Jiang, "A finite state model for respiratory motion analysis in image guided radiation therapy," Phys. Med. Biol. **49**, 5357–5372 (2004).
[40]H. Shirato, S. Shimizu, K. Kitamura, T. Nishioka, K. Kagei, S. Hashimoto, H. Aoyama, T. Kunieda, N. Shinohara, H. Dosaka-Akita, and K. Miyasaka, "Four-dimensional treatment planning and fluoroscopic real-time tumor tracking radiotherapy for moving tumor," Int. J. Radiat. Oncol., Biol., Phys. **48**, 435–442 (2000).